Developmental Cell
Article

SAM Domain Polymerization Links Subnuclear Clustering of PRC1 to Gene Silencing

Kyoichi Isono,[1,4,5,*] Takaho A. Endo,[2] Manching Ku,[6] Daisuke Yamada,[1] Rie Suzuki,[1] Jafar Sharif,[1] Tomoyuki Ishikura,[1] Tetsuro Toyoda,[3] Bradley E. Bernstein,[6] and Haruhiko Koseki[1,4,*]
[1]Laboratory for Developmental Genetics, RIKEN Center for Integrative Medical Sciences (IMS-RCAI)
[2]Laboratory for Integrative Genomics, RIKEN IMS-RCAI
[3]Advanced Center for Computing and Communication, RIKEN
[4]CREST, Japan Science and Technology Agency
[5]PREST, Japan Science and Technology Agency
1-7-22 Suehiro, Tsurumi-ku, Yokohama 230-0045, Japan
[6]Howard Hughes Medical Institute and Department of Pathology, Massachusetts General Hospital and Harvard Medical School, Boston, MA 02114, USA
*Correspondence: isono@rcai.riken.jp (K.I.), koseki@rcai.riken.jp (H.K.)
http://dx.doi.org/10.1016/j.devcel.2013.08.016

SUMMARY

The Polycomb-group (PcG) repressive complex-1 (PRC1) forms microscopically visible clusters in nuclei; however, the impact of this cluster formation on transcriptional regulation and the underlying mechanisms that regulate this process remain obscure. Here, we report that the sterile alpha motif (SAM) domain of a PRC1 core component Phc2 plays an essential role for PRC1 clustering through head-to-tail macromolecular polymerization, which is associated with stable target binding of PRC1/PRC2 and robust gene silencing activity. We propose a role for SAM domain polymerization in this repression by two distinct mechanisms: first, through capturing and/or retaining PRC1 at the PcG targets, and second, by strengthening the interactions between PRC1 and PRC2 to stabilize transcriptional repression. Our findings reveal a regulatory mechanism mediated by SAM domain polymerization for PcG-mediated repression of developmental loci that enables a robust yet reversible gene repression program during development.

INTRODUCTION

Polycomb group (PcG) proteins mediate heritable and reversible silencing of developmental genes to control cell proliferation, differentiation, developmental patterning, and organogenesis in metazoans (Satijn and Otte, 1999; Simon and Kingston, 2009; Sawarkar and Paro, 2010). PcG gene products form at least two distinct evolutionarily conserved multimeric protein complexes commonly known as the Polycomb repressive complex-1 (PRC1, which includes Mel18, Bmi1, Ring1A, Ring1B, Cbx2, Cbx4, Phc1, Phc2, etc. in mice) and complex-2 (PRC2, which includes Ezh2, Eed, and Suz12 in mice). PRC1 can be recruited to its target loci via two major pathways that are either dependent or independent on preexisting of H3K27 trimethylation (H3K27me3) marks. PRC2 mediates H3K27me3 deposition, and this may lead to sequential PRC1 binding (Cao et al., 2002). Recently, Kdm2b was proposed to recognize CpG islands and contribute to PRC1 recruitment independently of H3K27me3 (Farcas et al., 2012; Wu et al., 2013). Although these recent advances have significantly broadened our view on PcG targeting and regulatory networks, how PRC1 mediates gene repression remains poorly understood despite the fact that several mechanisms such as histone H2A monoubiquitination (Stock et al., 2007), compaction of chromatin (Francis et al., 2004; Grau et al., 2011), and regulation of higher order chromatin structure have been previously proposed (Eskeland et al., 2010).

PRC1 components cluster into microscopically visible speckles in *Drosophila* and mammals, designated as "PcG bodies." Several studies in *Drosophila* have suggested a role of PcG proteins in facilitating long-range gene repression by bringing distantly separated *cis*-regulatory Polycomb group responsive elements (PRE) into close spatial proximity (Bantignies et al., 2003; Vazquez et al., 2006). Through such interactions, PcG bodies could be involved in mediating silencing, presumably by regulating higher order chromatin structures (Buchenau et al., 1998; Lanzuolo et al., 2007; Bantignies et al., 2011). However, despite this proposed role for PcG bodies in PcG-mediated transcriptional silencing, to our knowledge at present there is no direct evidence that links the formation of PcG bodies to gene repression, partly because the precise molecular mechanisms that mediate PcG body formation are still unknown. PRC1 clustering and formation of PcG bodies in mammals have been studied mainly in immortalized tumor cell lines, in which PRC1 forms subnuclear speckles at pericentric heterochromatic regions (PCH) whereas the distribution of PRC1 in euchromatic regions (Saurin et al., 1998; Suzuki et al., 2002) appears to be relatively weak and uniform (Figure S1A available online). Electron microscopic observations revealed that in euchromatic regions, PRC1 is localized in the perichromatin compartment where transcriptionally active genes are present (Cmarko et al., 2003). In primary human fibroblasts, PRC1 exhibits a punctuated or granular distribution (Saurin et al., 1998).

However, these previous studies have not adequately described the detailed nature of the PRC1 clusters or the process of clustering and, as a result, the functional importance of PRC1 cluster formation in mammalian cells remains controversial.

One way to understand the function of the PRC1 clusters should be to experimentally perturb cluster formation and assess the impact on PRC1-mediated transcriptional silencing. Interestingly, previous biochemical studies have found several evolutionary conserved domains that could potentially mediate cluster formation or oligomerization of PRC1. The sterile alpha motif (SAM) domain observed in the *Drosophila* Polyhomeotic (Ph) and Sex-comb-midleg (Scm) proteins and their mammalian orthologs are particularly intriguing because they possess unique head-to-tail interaction capacity, which can cause the recombinant Ph-SAM domain to polymerize in vitro (Kim et al., 2002). Consistent with this observation, it has been suggested that a mammalian Ph ortholog Phc1 could be a critical PRC1 component for recruitment of a second nucleosomes into the recombinant mammalian Polycomb core complex (PCC) and nucleosomal template in vitro (Lavigne et al., 2004). Importantly, by overexpressing various mutant version of Ph in *Drosophila* wing disc, a recent study by Robinson et al. (2012) suggested the involvement of Ph-SAM polymerization in *AbdB* gene repression. However, the mechanisms underlying Ph-SAM polymerization-mediated gene silencing remain unclear.

In this study, we have focused on the question of whether and how PRC1 clustering mediates the repression of PcG target genes. By using several mutant alleles we have determined that the SAM domain of Phc2, a Ph ortholog, functions as an essential module to mediate PRC1 clustering. We demonstrated that the polymerization capacity of the Phc2-SAM domain is crucial for PRC1 clustering, stable binding of PRC1 and PRC2-mediated H3K27me3 at target genes and robust gene silencing activity. Our results will contribute to the revision/extension of current models of PcG-mediated gene silencing by demonstrating roles of the Phc2-SAM domain.

RESULTS

Subnuclear Clustering of PRC1 in Mouse Embryonic Fibroblasts

Because the precise mechanisms of PRC1 clustering in mammalian primary cells is not yet well understood, we set out to examine the subnuclear distribution of PRC1 in mouse embryonic fibroblasts (MEFs). Results of conventional immunofluorescent (IF) analyses using paraformaldehyde-fixed MEFs revealed that Ring1B, the catalytic subunit of PRC1, forms speckles in the nucleus together with other PRC1 components such as Mel18, Bmi1, Phc1, Phc2, and Cbx2 (Figure 1A; data not shown). Strikingly, different from previously published reports analyzing tumor cell lines, we observed that Ring1B clusters in MEF cells were significantly associated with H3K27me3 speckles but were excluded from the PCH regions demarcated by H3K9me3 (Figures 1B and S1A). We quantified the overlap between Ring1B and H3K27me3 speckles and compared this with the overlap with H3K27me2, H3K9me2, or acetylated histone H3 (H3ac) (Figure S1B). These analyses revealed that Ring1B clusters were preferentially associated with H3K27me3-enriched regions (Figure S1C). Importantly, similar subnuclear clustering of PRC1 and association with H3K27me3 speckles were also seen in mouse embryonic stem cells (ESCs) (Figure S1D) and fetal tissues (data not shown), suggesting that this pattern was not restricted to primary MEFs.

To investigate PRC1 clustering in live cells, we generated knockin (KI) mice expressing Mel18-EGFP or Ring1B-YFP fusion protein (Figures S1E and S1F). We first tested whether the respective fusion proteins could function normally like their endogenous counterparts. The *Mel18*$^{GFP/GFP}$ and *Ring1B*$^{YFP/YFP}$ mice were fertile and viable and did not exhibit posterior transformations of the axis, which is a common abnormality seen in PRC1 mutants (data not shown). Moreover, Mel18-EGFP and Ring1B-YFP proteins were properly expressed and formed biochemically-detectable complexes with other PRC1 proteins (Figures S1G and S1H), functionally indistinguishable from their untagged, wild-type counterparts. We observed that both fusion proteins formed clusters in MEFs and ESCs and confirmed their overlap with other PRC1 components (Figures 1C and S1I). Time-lapse imaging analysis using *Ring1B*$^{YFP/YFP}$ MEFs revealed maintenance of Ring1B-YFP clusters that were stable for at least 90 min (Figure 1D; Movie S1; data not shown). Based on these evidences, we concluded that PRC1 forms stable subnuclear clusters in MEFs. We next tested whether PRC1 components located within the PRC1 clusters undergo dynamic interchanges with the nonchromatin bound PRC1 pool as previously reported in *Drosophila* embryos and human cell lines (Hernández-Muñoz et al., 2005; Ficz et al., 2005). Indeed, after photobleaching of PRC1 clusters in *Ring1B*$^{YFP/YFP}$ MEFs, we found a rapid recovery of Ring1B-YFP fluorescence, reaching a plateau level at ~5 min (Figure 1E; Movie S1). This suggests that although PRC1 clusters are stably retained on chromatin, individual PRC1 components are dynamically interchanged.

PRC1 Clustering Correlates with Gene Silencing

To test whether PRC1 clusters represent silencing domains like the PcG bodies in *Drosophila*, we investigated whether known PRC1 target genes in mice associated with such clusters by immuno-DNA FISH (iFISH) with anti-GFP antibody in *Mel18*$^{GFP/GFP}$ MEFs. The iFISH analysis revealed intensive accumulation of PRC1 on canonical PcG target genes, including *Hoxb1*, *Hoxb7–9*, and *Cdkn2a* at 84% (37 out of 44), 78% (50 out of 64), and 73% (47 out of 64) of the respective loci (Figures 2A and 2B). Importantly, we also observed speckled accumulation of PRC1 at other *Hox* clusters and several known PcG targets such as *Pitx2* and *Meis2* (Figure S2A; data not shown). By contrast, such accumulation was barely detectable at a genomic region downstream of *Cdkn2a* (~200 kb away), where there was no H3K27me3 occupancy (8%; 5 out of 64 cells) (Figures 2A and 2B).

In *Drosophila* imaginal disc cells, two separate *Hox* gene loci are brought together to form PcG-mediated clusters (Bantignies et al., 2011). Similarly, in murine ESCs it has been shown that multiple *Hoxb* genes separated by hundreds of kilobases of DNA converge together in a Ring1B-dependent manner and that this juxtaposition is required for repressing transcription (Eskeland et al., 2010). Based on our observations in MEFs and ESCs, we hypothesized that the PRC1 clusters could be linked to condensation and repression of the *Hoxb* cluster. We then performed iFISH analysis and found that indeed *Hoxb1*,

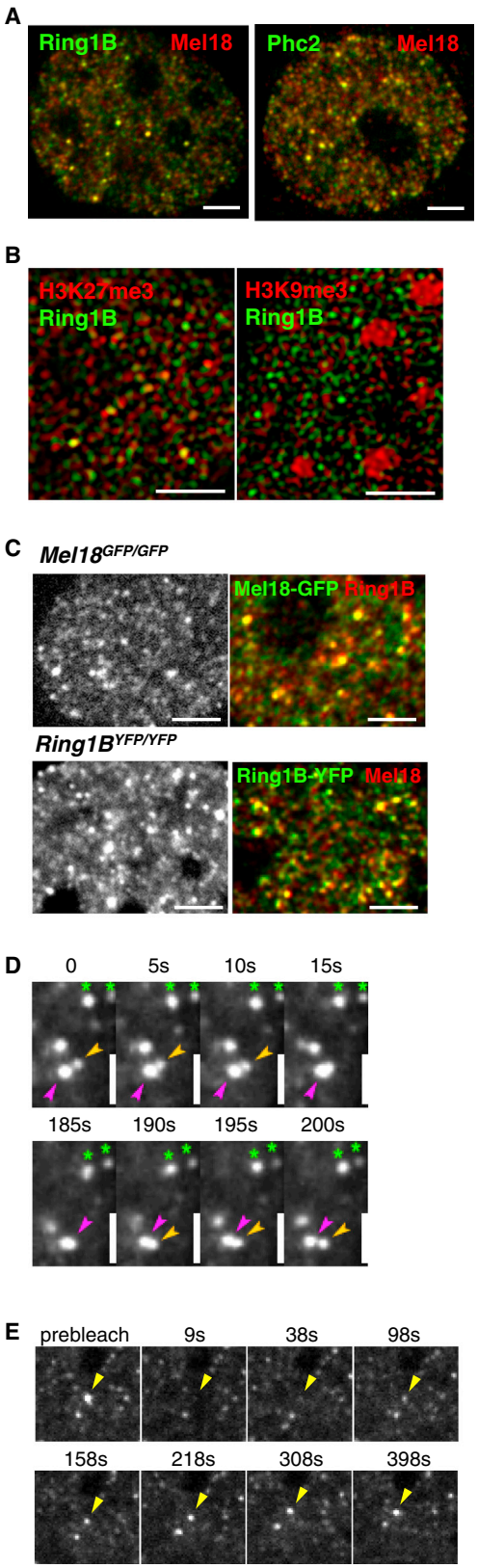

Figure 1. Subnuclear Clustering of PRC1 in Primary MEFs

(A) Subnuclear colocalization of Ring1B, Mel18, and Phc2 in MEFs. These PRC1 components form distinctive speckles (yellow parts). Scale bars represent 3 μm.

(B) Subnuclear distributions of Ring1B, H3K27me3, and H3K9me3 in MEFs (deconvolved images). Scale bars represent 3 μm.

(C) Subnuclear localization of Mel18-GFP or Ring1B-YFP fusion proteins in MEFs. Autofluorescence images for Mel18-GFP and Ring1B-YFP (left) and immunostained images (right) in *Mel18*$^{GFP/GFP}$ and *Ring1B*$^{YFP/YFP}$ MEFs. Scale bars represent 3 μm.

(D) Time-lapse images of *Ring1B*$^{YFP/YFP}$ MEFs. Most of Ring1B-YFP speckles (e.g., asterisks) were stable but some were moving as if they contacted (arrowheads, see Movie S1). Scale bars represent 1 μm.

(E) Constitutive exchange of Ring1B-YFP at the PRC1 clusters. A PRC1 cluster (arrowhead) in *Ring1B*$^{YFP/YFP}$ MEFs was subjected to photo-bleaching and subsequent sequential imaging.

See also Movie S1 and Figure S1.

Hoxb7–9, and *Hoxb13* genes, which occupy an ~280 kb genomic region, were condensed into a single cluster in MEFs (Figure 2C). Similarly, in ESCs we observed association of *Hoxb1* and *Hoxb7–9* in a single cluster (Figure S2B). Deletion of *Ring1B* in *Ring1A*-KO MEFs by ERT2-Cre-mediated recombination led to dissociation of *Hoxb1* and *Hoxb7–9* and derepression of transcription from these loci (Figures S2C–S2F). Collectively, these observations suggest that PRC1 clustering is associated with condensation and silencing of the *Hox* genes both in MEFs and ESCs.

Given the essential role for PcG proteins in development, we asked if such PRC1 clustering occurs during murine embryogenesis. Spatiotemporal expression patterns of *Hox* genes during axial development are known to correlate with their sequential order within each cluster (Kmita and Duboule, 2003; Deschamps and van Nes, 2005). We compared association of genomic regions around *Hoxb1* and *Hoxb13* with PRC1 clusters between cranial and caudal tissues. Tissues anterior to the otic vesicles ("Head" in Figure 2D) and tissues posterior to the forelimbs ("Tail") were dissected from 9.5 dpc *Mel18*$^{GFP/GFP}$ embryos, dissociated and spread on coverslips. To minimize experimental artifacts, we limited the culturing time to less than 16 hr after dissection. We observed that *Hoxb1*, *Hoxb2*, and *Hoxb3* were expressed at high levels in cells derived from the tail region compared to the head, whereas *Hoxb13* expression was hardly detectable in cells from either region (Figure 2D). iFISH analyses revealed that *Hoxb1* and *Hoxb13* were closely associated in single clusters in cells from the head region, whereas in cells from the tail region these signals were significantly separated (Figures 2E and 2F). Importantly, *Hoxb1* speckles were associated with the PRC1 clusters in the head region but not in the tail region whereas *Hoxb13* speckles showed association with PRC1 clusters both in the head and tail regions (Figures 2E and 2G). Taken together, these results indicate that PRC1 clustering is associated with gene repression.

The Role of Phc2-SAM Domain in PRC1 Clustering

Our above observations, together with previous reports in *Drosophila*, suggest that PRC1 clustering mediates gene repression; however, it is not known how the clusters form. We thus sought to identify the molecular modules that are involved in cluster formation. To this end, we focused on the SAM domain-containing Ph orthologs, because of the reason that

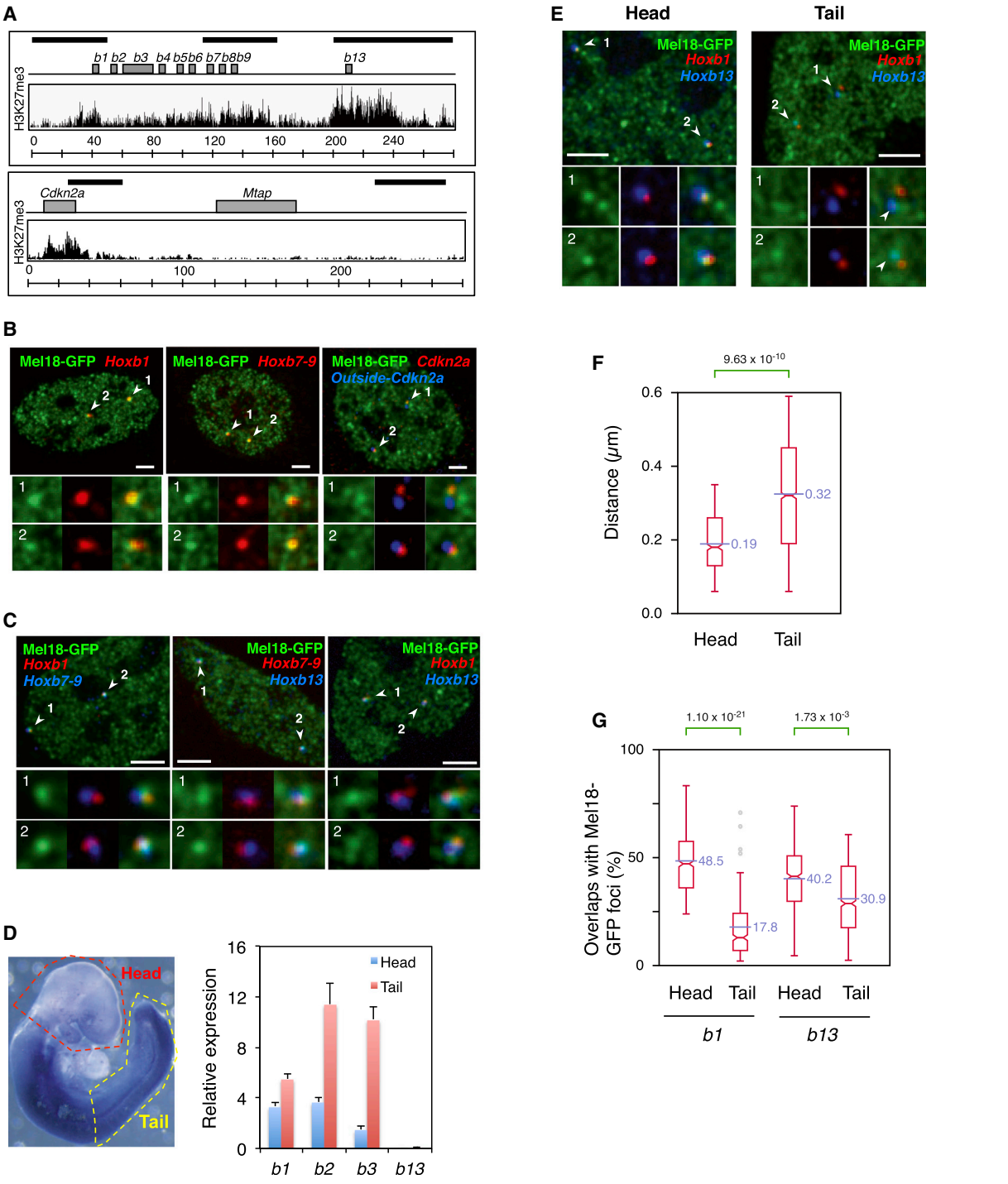

Figure 2. PRC1 Clustering at PcG Target Genes Correlates with Their Repression in MEFs and Embryos

(A) Distributions of H3K27me3 at the *Hoxb* and *Cdkn2a-Mtap* genomic regions. Shaded boxes and bold bars indicate genic regions and positions of FISH probes, respectively. Scale bars represent 2 μm.

(B) Association of *Hoxb1*, *Hoxb7–9*, and *Cdkn2a* regions with Mel18-GFP foci. The IF image for Mel18-GFP (green) is superimposed with FISH images for *Hoxb1* (red), *Hoxb7–9* (red), or *Cdkn2a* (red) and *Outside-Cdkn2a* (blue). *Outside-Cdkn2a* probe recognizes a genomic region ~200 kb distant from *Cdkn2a*. Higher magnification views for FISH signals indicated by arrowheads are shown below. Scale bars represent 2 μm.

(C) Condensation of the *Hoxb* gene cluster at a single PRC1 cluster. The IF image for Mel18-GFP (green) is superimposed with the FISH image for *Hoxb1* (red)/*Hoxb7–9* (blue), *Hoxb7–9* (red)/*Hoxb13* (blue), or *Hoxb1* (red)/*Hoxb13* (blue). Scale bars represent 3 μm.

(D) Expression of *Hoxb* genes in 9.5 dpc embryos. Whole mount in situ hybridization for *Hoxb3* (left). RT-qPCR (right) shows expression levels of *Hoxb* genes in MEFs derived from tissues anterior to the otic vesicles ("Head," red dotted line in the left panel) and tissues posterior to the forelimbs ("Tail," yellow dotted line). Each expression is normalized to that of *Gapdh*. Error bars represent 1 SD.

(legend continued on next page)

the head-to-tail polymerization capacity of SAM domain might bring PRC1 molecules into close spatial proximity.

By analogy to the SAM domain of Ph, previous studies have implied that the end-helix (EH) surface of the SAM domain of one Phc2 molecule would interact with the midloop/helix-3 (ML) surface of another, to facilitate SAM-mediated sequential polymerization and that a mutation (L307R) in the EH surface of the Phc2-SAM domain would impair SAM polymerization (Kim et al., 2002). To test impacts of the Phc2-SAM domain on PRC1 assembly, we transiently overexpressed wild-type (WT) or mutant (L307R) FLAG-tagged Phc2 with Myc-tagged Mel18, Ring1B, and Cbx2 in 293T cells and purified exogenously expressed PRC1 from nuclease digested lysates with FLAG M2 beads (Figures 3A and S3A). We observed that Myc-Mel18, Myc-Ring1B, and Myc-Cbx2 all coimmunoprecipitated with both FLAG-Phc2 (WT) and FLAG-Phc2 (L307R) to a similar extent (Figure 3B, FLAG-purified). This suggests that the SAM domain mutation does not primarily affect the interaction of Phc2 with Mel18, Ring1B, and Cbx2. Further, we compared the relative molecular weights of protein complexes associated with FLAG-Phc2 (WT) and FLAG-Phc2 (L307R) by sucrose gradient ultracentrifugation. Although the molecular weight of monomeric PRC1 was expected to be ~190 kDa, we found that FLAG-Phc2 (WT) or FLAG-Phc2 (L307R) complexes were distributed in fractions representing molecular weights larger than 669 kDa or the 200–669 kDa range, respectively (Figure 3B, brackets). Because the FLAG-purified complexes did not contain histone proteins (Figure S3B), such complex formation might not require nucleosomes as an association platform. This result indicates that the Phc2-SAM domain plays a role for PRC1 polymerization.

We went on to test the role of the Phc2-SAM domain in PRC1 clustering. We expressed GFP-tagged Phc2^{L307R} (GFP-Phc2^{L307R}) in U2OS cells. Consistent with our hypothesis, the mutant protein failed to cluster and significantly abolished the speckled accumulation of endogenous Ring1B at the PCH in transfected cells, whereas the wild-type GFP-Phc2 intensely colocalized with Ring1B (Figure 3C). To confirm that the polymerization activity and not some other cryptic function of the SAM domain regulate PRC1 clustering, we generated another version of Phc2 that is fused to GFP at the C terminus (Phc2-GFP) and its binding partner GST-SAM with either mutation L307R or L293R/H298R. The mutation L293R/H298R is located in a key position of the ML surface. Recombinant His-tagged Phc2-GFP was able to bind to the L293R/H298R SAM but not to the L307R SAM, indicating that the ML surface of His-Phc2-GFP is intact but the EH surface is abrogated by the GFP motif (Figures 3D and S3C). Similar to GFP-Phc2^{L307R}, exogenous expression of Phc2-GFP perturbed Ring1B clustering (Figure 3C). These findings support the involvement of the polymerization capacity of Phc2-SAM in PRC1 clustering.

In our model, SAM-mediated sequential polymerization via the EH-ML interaction is essential for PRC1 clustering. Based on this, exogenous EH mutant (GFP-Phc2^{L307R} or Phc2-GFP) would be able to interact with the EH surface of endogenous Phc2; however, due to the defect of the EH surface, it would not undergo the sequential polymerization, resulting in interfering endogenous Ring1B clustering (Figure 3C). If this hypothesis is true, mutation of both EH and ML surfaces of exogenous Phc2 will restore the clustering of endogenous PRC1, because the mutated protein will no longer be able to interact with the endogenous counterparts and thus would not exert the domain negative effect on PRC1 clustering. It should be noted that Phc2 is able to interact with Ring1B and Mel18 through its HD1 domain (Figures S3D and S3E), indicating that HD1-lacking Phc2 would be better to assess the direct impact on the SAM polymerization. To test our hypothesis, we performed triple Phc2 mutations, namely, deletion of the HD1 domain along with incorporating single (ML: L293R/H298R or EH: L307R) or double (ML and EH: H298R/L293R/L307R) surface disruption. As expected, each single mutant inhibited Ring1B clustering but the double surface mutants did not affect the clustering of endogenous Ring1B (Figure 3E). Taken together, subnuclear PRC1 clustering likely requires the polymerization capacity of Phc2-SAM.

Phc2-SAM Links PRC1 Clustering to Gene Silencing

To investigate the role of Phc2-SAM polymerization in PcG-mediated gene silencing, we generated KI alleles that express Phc2^{L307R} or Cerulean (a GFP variant) fusion to the C terminus of the SAM domain (Phc2^{Ce}) (Figure S4A). We first confirmed the expression of both mutant proteins and their association with PRC1 in KI homozygous embryos by using immunoprecipitation (IP)/western analysis. Phc2^{L307R} was expressed to a similar extent as the wild-type Phc2 (Figure S4B). Phc2^{L307R} and the wild-type Phc2 both formed complexes with Cbx2, Ring1B, and Mel18; moreover, the mutation did not interfere with Mel18/Cbx2, Mel18/Ring1B, or Ring1B/Cbx2 interactions. Phc2^{Ce} was also expressed and formed complexes with Ring1B at a level similar to the wild-type (Figure S4B). Therefore, we concluded that core complexes of PRC1 were properly formed and expressed in *Phc2*$^{L307R/L307R}$ and *Phc2*$^{Ce/Ce}$ embryos.

We then examined the impact of the *Phc2*^{L307R} and *Phc2*^{Ce} mutations on PRC1 clustering by using the respective MEFs and IF analysis. The speckled colocalization of Ring1B and Mel18 was barely detectable in either of the KI homozygous MEFs (Figure 4A, top). Consistently, Mel18-GFP had a granular rather than a speckled distribution in the *Mel18*$^{GFP/GFP}$; *Phc2*$^{L307R/L307R}$ MEFs (Figure 4A, bottom). Phc2^{Ce} also

(E) Dissociation of a transcriptionally active *Hoxb1* region from the PRC1 cluster. IF images for Mel18-GFP (green) are superimposed with FISH images for *Hoxb1* (red) and *Hoxb13* (blue) in cells from "Head" (left) and "Tail" (right) regions of 9.5-dpc embryos. *Hoxb1* dissociates from PRC1 clusters in tail-derived cells. Scale bars represent 3 μm.
(F) Distances between *Hoxb1* and *Hoxb13* signals in Head- and Tail-derived cells. The boxes indicate the median and interquartile range of the data from each of 67 loci of the head or tail cells. Values in the boxes represent each average distance. The statistical significance was determined by the two-tailed Student's t test.
(G) Quantitative comparison of overlapped volumes of PRC1 clusters with *Hoxb1* or *Hoxb13* region between Head- and Tail-derived cells. Percentages of overlaps of *Hoxb1* or *Hoxb13* speckles with Mel18-GFP speckles were calculated by using deconvolved images for 67 *Hoxb1* or *Hoxb13* loci of the Head or Tail cells. The p values determined by the two-tailed Student's t test are indicated above the box plot.
See also Figure S2.

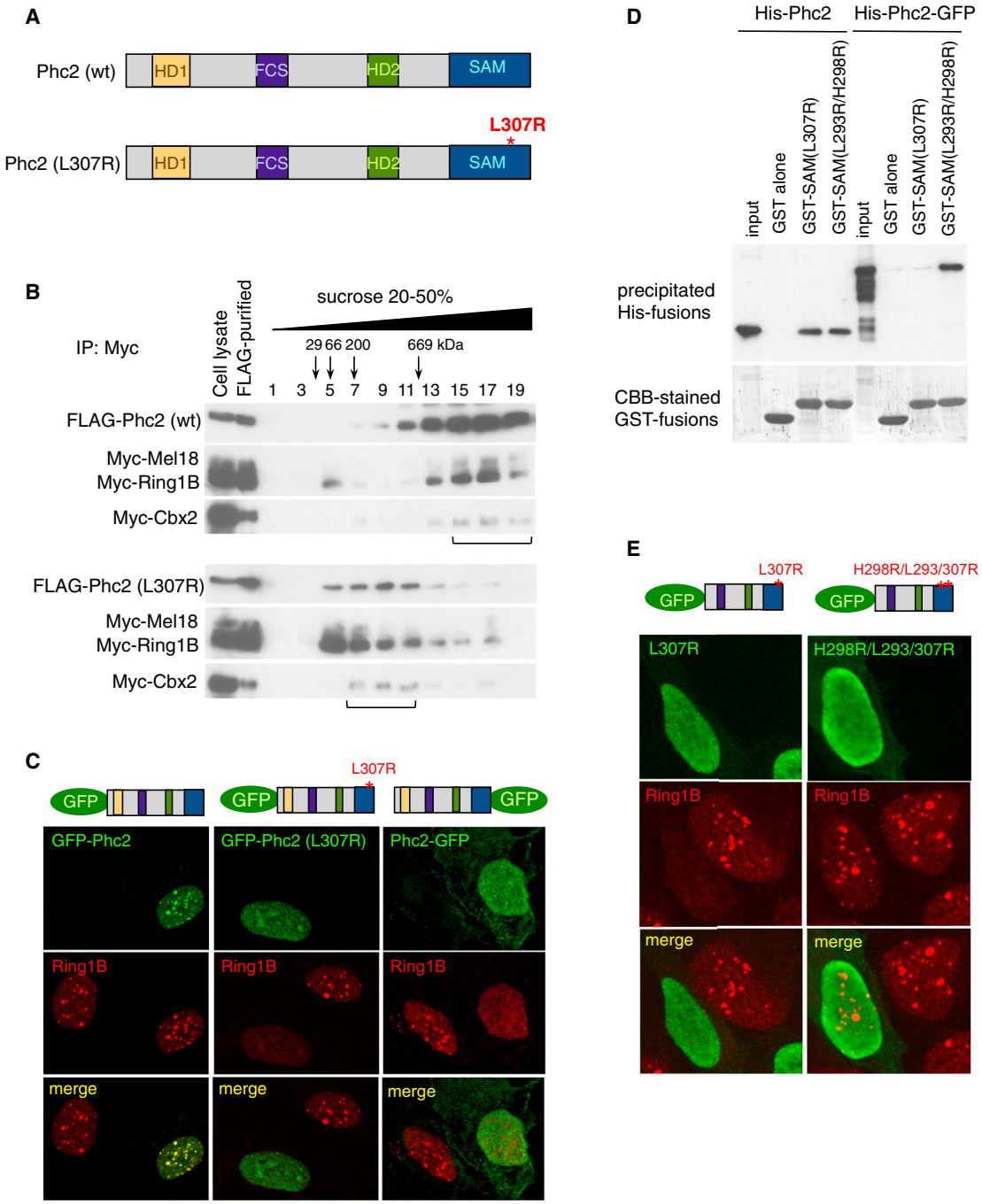

Figure 3. The Phc2-SAM Domain Mediates Clustering of PRC1 in Human Cell Lines

(A) Schematic representation for the 36 kDa isoform of Phc2, which is a developmentally major isoform of Phc2 (Yamaki et al., 2002). Four evolutionarily conserved domains, homology domain 1 (HD1), FCS zinc finger domain (FCS), homology domain 2 (HD2), and the SAM domain (SAM), are shown. The position of the L307R mutation is depicted.

(B) Sucrose gradient analysis of FLAG-purified Phc2 complexes in 293T cells. Every other fraction from a 20%–50% sucrose gradient was further isolated by using anti-Myc antibody, followed by immunoblotting with anti-FLAG or anti-Myc antibody.

(C) Subnuclear distribution of GFP-Phc2, GFP-Phc2 (L307R), or Phc2-GFP in U2OS cells. Cells transiently expressing the indicated constructs were immunostained with anti-GFP and anti-Ring1B antibodies.

(D) GST pull-down assay for recombinant His-tagged Phc2 (His-Phc2) and C-terminal GFP-fused Phc2 (His-Phc2-GFP) with GST-SAM-mutated fusion (L293R/H298R or L307R).

(E) Subnuclear distribution of a truncated Phc2 lacking HD1 and carrying a mutation only on the EH surface or mutations on both EH and ML surfaces in U2OS cells. Cells transiently expressing the indicated constructs were immunostained with anti-GFP and anti-Ring1B antibodies.

See also Figure S3.

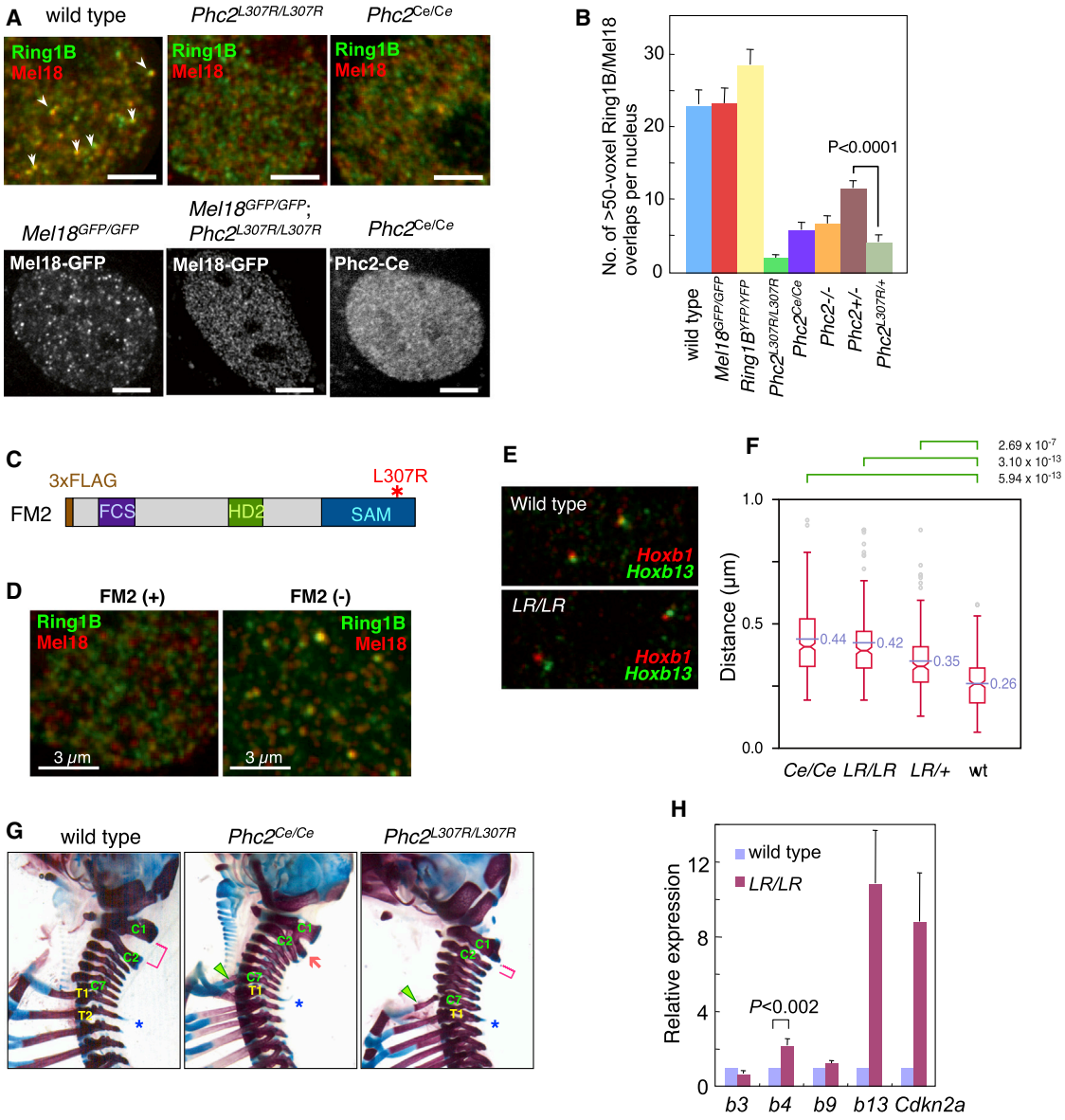

Figure 4. Polymerization Defect of Phc2-SAM Affects Subnuclear Clustering of PRC1 and *Hox* Gene Regulations

(A) Defects in PRC1 clustering in *Phc2* mutant MEFs. Typical PRC1 clusters in wild-type (arrowheads) are absent in $Phc2^{L307R/L307R}$ and $Phc2^{Ce/Ce}$ MEFs (top panels, immunostained images). Mel18-GFP in $Mel18^{GFP/GFP}$; $Phc2^{L307R/L307R}$ and Phc2-Cerulean in $Phc2^{Ce/Ce}$ exhibited a grainer distribution (bottom panels, live images). Scale bars represent 3 μm.

(B) Quantitative analysis for PRC1 clustering in wild-type and mutant MEFs. The number of >50-voxel Ring1B/Mel18 overlaps that represent degrees of PRC1 clustering were computationally enumerated in wild-type (n = 10), $Mel18^{GFP/GFP}$ (n = 11), $Ring1B^{YFP/YFP}$ (n = 11), $Phc2^{L307R/L307R}$ (n = 9), $Phc2^{Ce/Ce}$ (n = 10), $Phc2^{-/-}$ (n = 13), $Phc2^{+/-}$ (n = 9), and $Phc2^{L307R/+}$ (n = 9). Note that the >50-voxel Ring1B/Mel18 overlaps in $Phc2^{L307R/+}$ were significantly reduced compared with those of $Phc2^{+/-}$ MEFs ($p < 0.0001$ by two-tailed Student's t test). Error bars represent SEM.

(C) Schematic representation of FM2 version of Phc2, in which the HD1 domain is replaced with a triple FLAG tag and the L307R mutation is introduced.

(D) Immunostaining for Ring1B and Mel18 in MEFs expressing FM2 (+) or not (–).

(E) Representative images of two-color DNA-FISH for *Hoxb1* and *Hoxb13* in wild-type and $Phc2^{L307R/L307R}$ MEFs.

(F) Quantitative analysis for distances between *Hoxb1* and *Hoxb13* signals in $Phc2^{Ce/Ce}$ (Ce/Ce, n = 75), $Phc2^{L307R/L307R}$ (LR/LR, n = 103), $Phc2^{L307R/+}$ (LR/+, n = 148), and wild-type (WT) MEFs (WT, n = 85). The boxes indicate the median and interquartile range. Values in the boxes represent each average distance. The statistical significance was determined by the two-tailed Student's t test.

(G) Posterior transformations of the axial skeleton in $Phc2^{Ce/Ce}$ and $Phc2^{L307R/L307R}$ mice. Note the presence of an ectopic rib associated with the C7 vertebra in both mutants (green arrowheads) and that prominent spinous process characteristic of the T2 vertebra in wild-type were often seen associated with T1 in the mutants (asterisks). The C1 vertebra transformed partially to the C2 vertebra in $Phc2^{Ce/Ce}$ (red arrow) and almost perfectly in $Phc2^{L307R/L307R}$ (red bracket).

(H) Derepression of *Hoxb4*, *Hoxb13*, and *Cdkn2a* in $Phc2^{L307R/L307R}$ MEFs in RT-qPCR. Error bars represent SD. Expression levels are normalized to that of *Gapdh*.

See also Figure S4 and Table S1.

demonstrated a granular distribution. These results were further confirmed by quantitative analysis of the Ring1B/Mel18 overlap. We found that the number of >50-voxels Ring1B/Mel18 overlaps were significantly reduced in both KI homozygotes (Figure 4B). Moreover, PRC1 clustering was more severely affected in *Phc2*$^{L307R/+}$ than in *Phc2*$^{+/-}$ MEFs (Figure 4B), suggesting a dominant negative effect of Phc2^{L307R} upon PRC1 clustering. We thus rigorously tested this issue by using another KI allele that expresses FLAG-tagged mutant Phc2 (FM2) from the *rosa26* locus after Cre recombinase-mediated removal of the stop cassette (Figure S4C). Because FM2 harbors the L307R mutation and also lacks the HD1 region (Figure 4C), this mutant is expected to interact with PRC1 via the intact ML surface of its SAM domain. The expression of FM2 should, therefore, exclusively impair Phc2-SAM-mediated polymerization of PRC1 without changing the expression level of endogenous PRC1. We found that FM2 expression did not affect the overall expression level of PRC1 and FM2 normally associated with endogenous PRC1 (Figure S4D). Despite the unchanged expression levels of PRC1, we observed that FM2-expression induced defects specifically in PRC1 clustering (Figures 4D and S4E). On the basis of this evidence, we concluded that Phc2-SAM contributes to PRC1 clustering via its polymerization capacity. This model prompted us to hypothesize the involvement of other homologous SAM-domain proteins such as Phc1 and Phc3 in PRC1 clustering. Phc1 indeed intensively colocalizes with Phc2 in MEFs (Figure S4F) and we have previously reported that Phc1 interacts with Phc2 in developing embryos (Isono et al., 2005). Consistently, we observed that the speckled colocalization of Phc1 with Mel18 was considerably impaired in *Phc2*$^{L307R/L307R}$ MEFs (Figure S4F). Moreover, the expression of a mutant Phc1 having SAM-polymerization defects abolished the speckled clustering of Ring1B in U2OS cells to a similar extent of GFP-Phc2^{L307R} (data not shown). Taken together, SAM-domains of Phc2 and Phc1 (and presumably Phc3) synergistically contribute to PRC1 clustering likely through homophilic and heterophilic interactions.

We went on to examine the impact of Phc2-SAM polymerization on the condensation of the *Hoxb* gene cluster. We observed significant separation of *Hoxb1* and *Hoxb13* in *Phc2*$^{Ce/Ce}$ and *Phc2*$^{L307R/L307R}$ mutant MEFs, 0.42 μm and 0.44 μm, respectively, compared to 0.26 μm in wild-type (Figures 4E and 4F). Consistent with the defective PRC1 clustering (Figure 4B), we also observed de-condensation of the *Hoxb* gene cluster in *Phc2*$^{L307R/+}$ MEFs. These results indicated that the polymerization capacity of the Phc2-SAM domain is required for *Hoxb* condensation. We then asked whether the Phc2-SAM polymerization is required for repressing PRC1 target genes. Because PRC1 is involved in axial specification through the repression of *Hox* expression, we first determined if the axial skeletal development was affected in the absence of functional Phc2-SAM domain. We found obvious posterior transformations of the axis in *Phc2*$^{L307R/L307R}$ and *Phc2*$^{Ce/Ce}$ mice, as is also seen in *Phc2*$^{-/-}$ mice (Figure 4G; Table S1). Such changes were also observed in *Phc2*$^{L307R/+}$, *Phc2*$^{Ce/+}$ and FM2 transgenic mice (Table S1). Consistently, we found significant derepression of *Hoxb4* and *Hoxb13* in *Phc2*$^{L307R/L307R}$ MEFs, whereas *Hoxb3* and *Hoxb9* were unaffected (Figure 4H). Taken together, these studies implicated that Phc2-SAM polymerization is required for PRC1 clustering, chromatin condensation, and the repression of *Hoxb* genes. We also observed derepression of *Cdkn2a*, a solitary PRC1 target gene, and a clear increase of its products p19^{Arf} and p16^{Ink4a} in the KI mutants (Figures 4H and S4G). This observation for *Cdkn2a* suggests that gene condensation mediated by Phc2-SAM polymerization might not be the primary process of PRC1-mediated gene repression. Together with the role of Phc2-SAM in clustering of PRC1, we assume that Phc2-SAM polymerization mainly mediates PRC1 clustering at individual targets, which should be a prerequisite for gene condensation at clustered PRC1 target genes.

To test our model, we identified Ring1B and H3K27me3 target genes in MEFs by chromatin IP (ChIP) followed by DNA sequencing (ChIP-seq). We observed 769 and 4,338 genes bound by Ring1B and H3K27me3, respectively. A large subset of Ring1B target genes overlapped with H3K27me3 in a manner similar to ESCs (Figures S5A and S5B). Although we found a small group of genes exclusively bound by Ring1B, we could not confirm this result by locus specific ChIP-qPCR analysis, suggesting that some genes included in this group might be false positive signals (Figure S5C). Based on these ChIP-seq data, genes were classified into three groups: Ring1B+H3K27me3+, Ring1B-H3K27me3+, and Ring1B-H3K27me3−. We found that the average expression level of Ring1B+H3K27me3+ genes was significantly lower than the rest, based on the RNA-seq data (Gene Expression Omnibus [GEO] accession number GSM929719) (Figure S5D). These results indicate that, similar to ESCs, the co-occupancy by Ring1B and H3K27me3 is crucial for gene repression in MEFs. On the basis of these evidences, we focused on Ring1B+H3K27me3+ genes to investigate the role of the Phc2-SAM domain for gene repression. We observed that Ring1B+H3K27me3+ genes exhibited the highest degree of derepression in *Phc2*$^{L307R/L307R}$ MEFs, but, the level was subtle (Figure S5E). Further investigation on Ring1B+H3K27me3+ genes revealed that 12% of them exhibited robust and significant derepression in *Phc2*$^{L307R/L307R}$ MEFs (Figure 5A). These observations suggest that the Phc2-SAM-dependence may be regulated in a gene-specific manner. For example, clustered genes such as *Hox* could be more amenable to Phc2-SAM mediated repression. However, we observed that other Ring1B target loci that were within 100 kb genomic proximity of significantly derepressed Ring1B+H3K27me3+ genes in *Phc2*$^{L307R/L307R}$ MEFs were not derepressed (Figure 5B, left). Consistent with this, binding of CTCF, which could contribute to long-range interaction, was not altered between derepressed and unchanged genes (Figure 5B, middle). Instead, we found that RNA polymerase II was significantly excluded from genes repressed in Phc2-SAM-dependent manner (Figure 5B, right). We therefore propose that the polymerization capacity of Phc2-SAM is primarily active for local repression of individual target genes by regulating chromatin structure to facilitate exclusion of RNA polymerase II.

Phc2-SAM Polymerization Facilitates Local PRC1/PRC2 Engagement

We went onto investigate how Phc2-SAM polymerization regulates the local chromatin structure. We performed ChIP-seq for PRC1 (Ring1B) and observed obvious reduction in *Phc2*$^{L307R/L307R}$ MEFs at the *Hoxb* gene cluster and the *Cdkn2a* gene locus, which we validated by ChIP-qPCR analysis (Figures

5C and 5D). We next examined average changes in local binding of Ring1B between *Phc2*$^{L307R/L307R}$ and wild-type MEFs for Ring1B+H3K27me3+, Ring1B-H3K27me3+, and Ring1B-H3K27me3− genes. We found considerable and significant reduction of Ring1B binding only at Ring1B+H3K27me3+ genes (Figure 5E). In addition, we tested local binding of Mel18, another crucial PRC1 component, because of the reason that PRC1-related complexes (known as noncanonical PRC1) include Ring1B (Tavares et al., 2012; Gao et al., 2012). We found that Mel18 binding was decreased as well in *Phc2*$^{L307R/L307R}$ MEFs (Figure S5F). Taken together, we suggest a role for Phc2-SAM to facilitate stable target binding of PRC1.

We further checked the local activity of PRC2 because knocking out Ring1B leads to a local reduction of H3K27me3 at PRC1 target genes in ESCs (Endoh et al., 2008). We indeed observed a significant reduction of H3K27me3 at Ring1B+H3K27me3+ genes in *Phc2*$^{L307R/L307R}$ MEFs (Figures 5C, 5D, and 5F). This was accompanied with considerable decrease of PRC2 (Ezh2 and Suz12) binding (Figure S5F). Intriguingly, the Ring1B-H3K27me3+ gene category also showed subtle but significant reduction of H3K27me3 (Figure 5F). This might be due to the possibility that the H3K27me3 levels in these loci could be established by very low PRC1 level that we could not detect by ChIP-seq. We thus suggest a secondary role for Phc2-SAM to facilitate stable target binding of PRC2.

Finally, we examined the local accumulation of Ring1B and H3K27me3 upon FM2 overexpression in MEFs by ChIP-qPCR analysis and observed a similar reduction in Ring1B and H3K27me3 binding at *Hoxb* and *Cdkn2a* genes (Figure S5G). In summary, Phc2-SAM polymerization primarily plays a role for stable binding of PRC1 to the Ring1B+H3K27me3+ loci. Local chromatin structure mediated by Phc2-SAM polymerization of PRC1 may in turn promote the deposition of the H3K27me3 mark at least partly by stabilizing PRC2 binding.

DISCUSSION

In this report, we show that microscopically visible subnuclear PRC1 domains represent SAM polymerization-dependent PRC1 clustering at PcG target genes and that such clustering appears to be closely related to their gene silencing activity in mammalian cells. Further, PRC1 clustering itself is stable, but the participating PRC1 components within such foci are continuously interchanged with the PRC1 reservoir outside the clusters. We therefore propose that the SAM-mediated interaction likely contributes to capture and/or retainment of PRC1 at the target loci by counteracting the constitutive exchange of PRC1 components to and from the clusters (Figures 6A and 6B). Our data further point to a role of SAM domain-mediated PRC1 clustering to form chromatin configurations that are fit for stable binding of PRC1 and PRC2 and exclusion of RNA polymerase II. Importantly, a previous structural study revealed a capacity for the Ph-SAM domain to form head-to-tail helices with 6-fold screw symmetry, which could be necessary for the outward positioning for the rest of the Ph protein from the polymer axis (Kim et al., 2002). The same structural capacity could be possessed by SAM-domains of Phc2, Phc1, and Phc3 as well, as predicted by sequence homology. We speculate that multivalency and periodicity of PRC1 conferred by SAM-mediated polymerization play a key role to reinforce the PRC1/nucleosome interaction suitable for gene silencing (Figure 6C). The periodic nature of the polymerized PRC1 by SAM-mediated interactions may contribute to nucleosome alignment at regular intervals by the chromodomain/H3K27me3 interaction. This may in turn facilitate the organization of an optimum nucleosome density that is preferable for binding and biochemical activity of PRC2 (Yuan et al., 2012). Through these multiple and diverse mechanisms, SAM-mediated PRC1 clustering likely strengthens the PRC1/PRC2 interaction to yield robustly repressed chromatin landscapes, which efficiently blocks the access of RNA polymerase II and preventing chromatin remodeling (Figure 6C). It is also noteworthy that only 12% of Ring1B+H3K27me3+ genes exhibited robust and significant de-repression in *Phc2*$^{L307R/L307R}$ MEFs, despite the dominant negative function of Phc2^{L307R}. This observation implies that although Phc2-SAM polymerization could be a key mechanism for stable PRC1 binding and/or to silence PcG target genes, this process is complemented and buffered by other silencing mechanisms embedded in the PRC1 circuitry such as the H2A monoubiquitination (Endoh et al., 2012). We also speculate the role of Phc1-SAM and Phc3-SAM, which are closely related to Phc2-SAM, to aid in PRC1 cluster formation and gene silencing, because Phc1 is shown to colocalize with Phc2 at PRC1 clusters and synergistically regulate the repression with Phc2 (Figure S4F) (Isono et al., 2005).

Although SAM polymerization could be a critical process for silencing of PcG target genes, its contribution to the long-range interactions of separate PRC1-binding sites is still controversial. Although we showed that defective Phc2-SAM polymerization affects condensation of the *Hoxb* cluster, our data did not exclude the possibility that this condensation defect could be due to altered local chromatin as we have discussed above. It is, however, fascinating to speculate that the multivalency of polymerized PRC1 might yield a large amount of hypothetically free/exposed chromodomain motifs that could be used to bind to a second array of target chromatin (Figure 6D). This model is consistent with a previous observation (Lavigne et al., 2004) that PCC1-bound chromatin could recruit and repress a second nucleosomal array. Interestingly, they found that Phc1 plays a critical role in this recruitment process. Based on these findings, we propose that SAM-mediated PRC1 polymerization could also be used for propagation of silencing by facilitating the binding of PRC1 to a second chromatin array and that this process might play an essential role in PRC1- (and PRC2-) mediated transcriptional silencing, especially for genes that are located within multiple gene clusters such as the *Hox* loci.

The stable existence and/or maintenance of PRC1 clusters despite the dynamic and continuous exchange of PRC1 components suggests that Phc2-SAM polymerization should be accompanied by, and balanced with, its depolymerization at these clusters (Figures 6B and 6C). This depolymerizing effect may potentially contribute to keeping PcG repression reversible in response to developmental cues (Sawarkar and Paro, 2010). Indeed, activation of *Hox* cluster genes by developmental inputs is accompanied by decondensation of the cluster in ESCs and developing tissues (Chambeyron and Bickmore, 2004; Chambeyron et al., 2005; Eskeland et al., 2010). Consistent with this model, Phc2 itself has been closely linked to developmental signals. Phc2 interacts with MAPK activated kinases at subnuclear

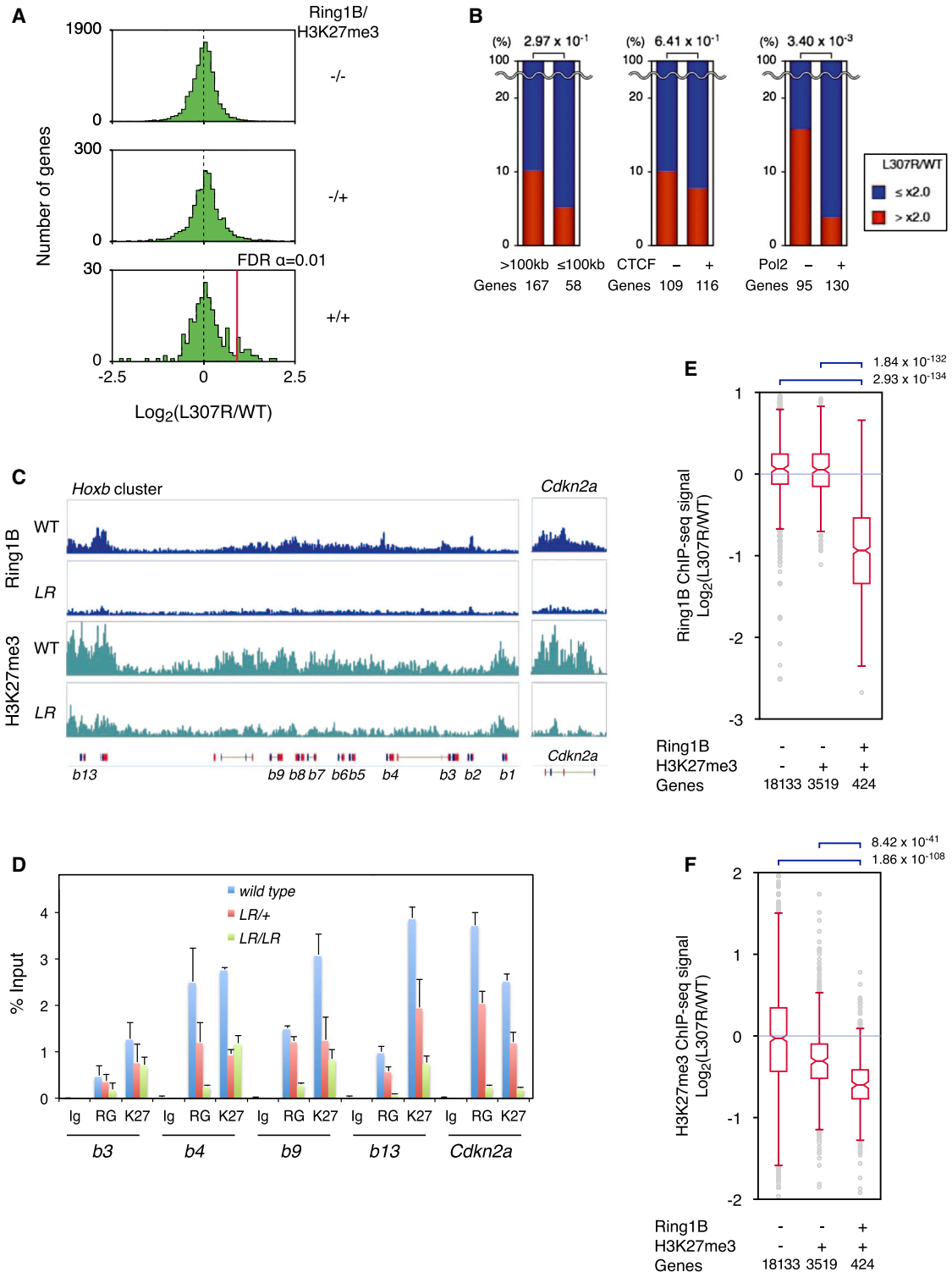

Figure 5. Phc2-SAM Polymerization Contributes to Stable Ring1B Binding and H3K27me3 Deposition at Ring1B+H3K27me3+ Genes and Their Repressions

(A) Significant derepression of a part of Ring1B+H3K27me3+ genes in *Phc2*$^{L307R/L307R}$ MEFs. Changes in gene expression in *Phc2*$^{L307R/L307R}$ MEFs are shown by histogram in each group. To detect derepressed genes in *Phc2*$^{L307R/L307R}$ MEFs, the distribution of gene expression change was fitted with one or two Gaussian distribution. The number of applied Gaussian distributions was determined with the lowest Bayesian information criterion (BIC). The threshold for derepressed genes (indicated by a red line) was selected where the number of genes in upper distribution became more than 99% (false discovery rate $\alpha = 0.01$) of genes.

(legend continued on next page)

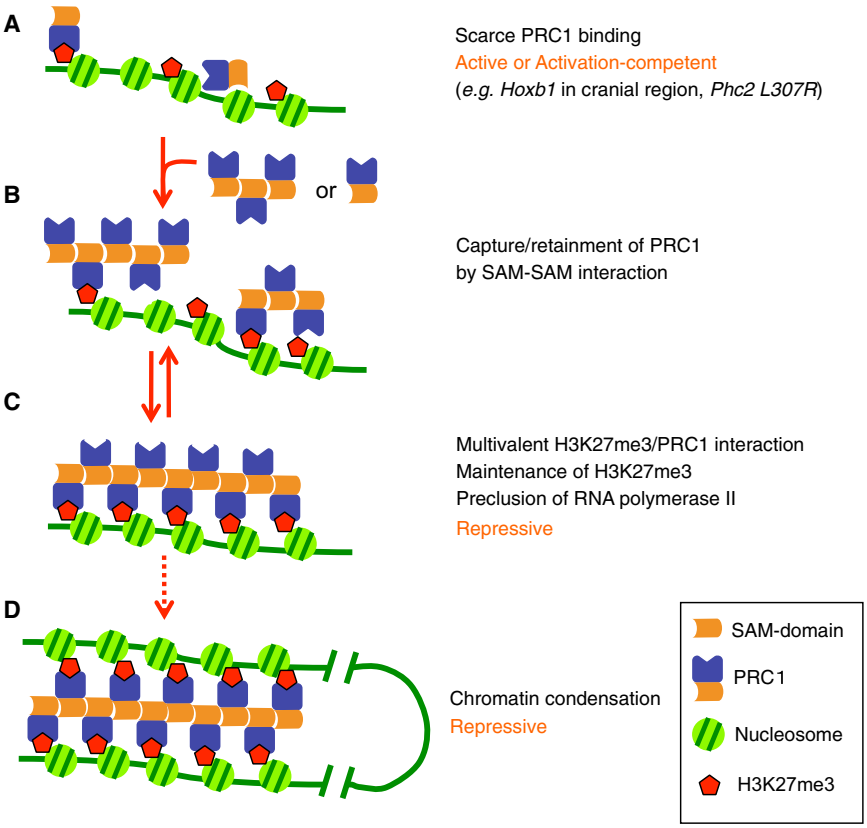

Figure 6. A Model for SAM Domain-Mediated Gene Repression

(A) Hypothetical PRC1 status at active or activation-competent chromatin.

(B) Capture and/or retainment of more PRC1 by SAM-mediated interactions at target genes.

(C) Stabilization of PRC1/nucleosome interaction through multivalent recognition of H3K27me3 by polymerized PRC1 via SAM-SAM interaction. PRC1 is dynamically exchanged even in this status. This chromatin status is also optimized for PRC2 binding and activity and preclusion of RNA polymerase II.

(D) Recruitment of another nucleosomal array to PRC1/nucleosome complexes by using free/vacant docking sites of PRC1 to mediate chromatin condensation as observed at *Hoxb* genes cluster.

PcG foci and is likely involved in mediating MAPK signals that maintain hematopoietic stem cells (Schwermann et al., 2009). Collectively, we propose that Phc2-SAM polymerization is involved in conferring robustness yet reversibility to PRC1-mediated repression of developmental genes that enables successful and robust implementation of developmental programs at PcG target loci.

EXPERIMENTAL PROCEDURES

Mice and Skeletal Analysis

A detailed description of the generation of the five different targeted mice, *Mel18*^{GFP}, *Ring1B*^{YFP}, *Phc2*^{Ce}, *Phc2*^{L307R}, and ROSA26-flag-tagged Phc2 L307R (FM2) is in the Supplemental Experimental Procedures. Skeletal phenotypes of newborns were analyzed as described previously (Kessel and Gruss, 1991). All animal experiments were carried out according to the in-house guidelines for the care and use of laboratory animals of the RIKEN, Yokohama Institute, Japan.

Immunoprecipitation

To prepare whole cell extracts, a single 11.5 days postcoitum (dpc) embryo was sonicated in 400 μl of 250 mM NaCl-IP buffer (20 mM HEPES [pH 7.8], 10% [v/v] glycerol, 250 mM NaCl, 0.2 mM EDTA, 1 mM DTT) containing 4 mM Pefabloc SC (Roche) and insoluble materials were removed by centrifugation. The whole cell extract was precleared with 50 μl of 50% (v/v) protein G-Sepharose at 4°C for 60 min and then incubated with protein G-Sepharose bound with appropriate antibodies for 90 min. Protein-bound protein G-Sepharose was washed with 800 μl of the 250 mM-IP buffer five times, boiled in SDS-sample buffer, and separated on 9% denaturing polyacrylamide gels followed by western blot analysis.

iFISH

MEFs on coverslips were fixed with 4% paraformaldehyde (PFA) and were subjected to immunostaining with anti-GFP antibody as a primary antibody and then the secondary antibody Alexa 647 as described (Miyagishima et al., 2003). Subsequently, DNA-FISH was carried out on the immunostained cells as previously described (Solovei et al., 2002). Detailed descriptions for immunostaining and DNA-FISH are in the Supplemental Experimental Procedures.

Imaging

All images were collected by using a high-speed spinning disc confocal unit (CSU-X1, Yokogawa Electric) equipped with a cooled CCD camera

(B) Preclusion of RNA polymerase II from a subset of Ring1B+H3K27me3+ genes in *Phc2*$^{L307R/L307R}$ MEFs. Ring1B+H3K27me3+ genes (225 genes) significantly derepressed in *Phc2*$^{L307R/L307R}$ MEFs was investigated based on genomic configuration (left; association of other Ring1B+H3K27me3+ genes within 100 kb genomic region), CTCF binding (middle), or RNA polymerase II binding (right) (Stamatoyannopoulos et al., 2012). Number of genes in each group is shown at the bottom. Frequency of genes derepressed in *Phc2*$^{L307R/L307R}$ MEFs is indicated by red columns. Statistical significance was estimated by using χ^2 test. CTCF, GEO accession number GSM918743; RNA polymerase II, GEO accession number GSM918761.

(C) Read density for Ring1B and H3K27me3 ChIP-seq libraries at the *Hoxb* gene cluster and *Cdkn2a* in wild-type (WT) and *Phc2*$^{L307R/L307R}$ (*LR*) MEFs. Known transcripts (red/blue) are indicated. The y axis represents ChIP-seq signal.

(D) ChIP-qPCR analysis of Ring1B (RG) and H3K27me3 (K27) for *Hoxb* genes and *Cdkn2a* in wild-type, *Phc2*$^{L307R/+}$ (*LR*/+), and *Phc2*$^{L307R/L307R}$ (*LR*/*LR*). Error bars represent 1 SD.

(E) Significant reduction in Ring1B binding in Ring1B+H3K27me3+ genes. The boxes indicate the median and interquartile range. The statistical significance was determined by the two-tailed Student's t test.

(F) Significant reduction in H3K27me3 binding in Ring1B+H3K27me3+ genes. The boxes indicate the median and interquartile range. The statistical significance was determined by the two-tailed Student's t test.

See also Figure S5.

(ORCA-AR, Hamamatsu Photonics). For details, see the Supplemental Experimental Procedures.

Computational 3D-Image Analysis

Images with 65 nm pixels in X-Y and 300-nm steps in Z were deconvolved one iteration with AutoDeblur/AutoVisualize software (AutoQuant Imaging). Deconvolved images along the z axis were analyzed with Volocity[3] software (Improvision). Regions-of-interest (ROIs) of PcG protein signals and those *Hoxb1/13* FISH signals were selected by a criterion with an SD of value 4 and a criterion with an SD of value 10, respectively. Overlapping volumes between these ROIs were calculated arithmetically. In the analysis between Ring1B and modified histone H3, individual ROIs were selected by a threshold of intensity giving their maximum number of 200 or a little more and then the top 200 were subjected to the colocalization calculation. Two-point distances between centers of individual FISH signals were measured using Volocity[3].

GST Pull-Down Assay

Recombinant GST-fusions expressed in *Escherichia coli* were purified with glutathione Sepharose 4B, and the complexes were directly incubated with target proteins. Precipitated targets were detected by immunoblotting with appropriate antibodies. For details, see the Supplemental Experimental Procedures.

Microarray and Data Analysis

Wild-type and *Phc2*$^{L307R/L307R}$ MEFs were used for RNA extraction and hybridization on GeneChip Mouse Genome 430 2.0 arrays (Affymetrix). Expression data were processed using the Affymetrix MAS5 algorithm with the BioConductor package running on R (http://www.bioconductor.org/). Signals were normalized using quantile normalization and compared between wild-type and mutant cells. Only genes having significant intensity in at least one of the wild-type and mutant were counted and the expression ratio was averaged when a gene had multiple assigned probes in the microarray design.

ChIP-Sequencing

MEFs were derived from wild-type or *Phc2*$^{L307R/L307R}$ littermate embryos at 12.5 dpc and directly cultured until reaching appropriate cell counts. Cells were fixed with 4% PFA for 10 min and used for ChIP-seq with anti-Ring1B or H3K27me3 antibodies. For H3K27me3, MEFs (1×10^6) were used in this assay as described previously (Ku et al., 2008). For Ring1B, MEFs (1×10^8) were sonicated using a Sonics Vibracell VCX 130 processor with a 3 mm stepped microtip in a volume of 300 μl of 150 mM NaCl-RIPA buffer for 20 s × 9 pulses at 30% amplitude. Cell extracts were subjected to immunoprecipitation with Ring1B antibody (300 μl)-coupled protein A/G magnetic beads (50 μl, Pierce) as described above. Eluted DNA samples were sheared using a Covaris S220 at 300 bp shearing. Libraries were prepared according to Illumina's instructions accompanying the NEBNext ChIP-Seq Library set (NEB E6200) and quantified by Qubit (Invitrogen), and their sizes were confirmed by Bioanalyzer (Agilent). Libraries were sequenced using Illumina HiSeq1000. Sequenced tags were mapped to the mouse genome (mm9) with the computer program Bowtie (http://bowtie-bio.sourceforge.net/index.shtml).

ACCESSION NUMBERS

Microarray and ChIP-seq data in this study were submitted to NCBI Gene Expression Omnibus (https://www.ncbi.nlm.nih.gov/geo/) under accession numbers GSE37346, GSE37530, and GSE42801.

SUPPLEMENTAL INFORMATION

Supplemental Information includes Supplemental Experimental Procedures, five figures, one table, and one movie, and can be found with this article online at http://dx.doi.org/10.1016/j.devcel.2013.08.016.

ACKNOWLEDGMENTS

We would like to thank Drs. S. Kobayakawa, K. Abe, M. Vidal, W. Bickmore, and T. Kamijo for the reagents used in this study. We also thank M. Kumon and M. Fujita for help this work. This work was supported by Grants-in-Aid for Scientific Research and for Scientific Research (to K.I. and H.K.) from the Ministry of Education, Culture, Sports, Science and Technology of Japan and PRESTO (to K.I.) and CREST (to H.K.) programs of Japan Science and Technology Agency.

Received: February 18, 2013
Revised: June 29, 2013
Accepted: August 19, 2013
Published: September 30, 2013

REFERENCES

Bantignies, F., Grimaud, C., Lavrov, S., Gabut, M., and Cavalli, G. (2003). Inheritance of Polycomb-dependent chromosomal interactions in Drosophila. Genes Dev. *17*, 2406–2420.

Bantignies, F., Roure, V., Comet, I., Leblanc, B., Schuettengruber, B., Bonnet, J., Tixier, V., Mas, A., and Cavalli, G. (2011). Polycomb-dependent regulatory contacts between distant Hox loci in Drosophila. Cell *144*, 214–226.

Buchenau, P., Hodgson, J., Strutt, H., and Arndt-Jovin, D.J. (1998). The distribution of polycomb-group proteins during cell division and development in Drosophila embryos: impact on models for silencing. J. Cell Biol. *141*, 469–481.

Cao, R., Wang, L., Wang, H., Xia, L., Erdjument-Bromage, H., Tempst, P., Jones, R.S., and Zhang, Y. (2002). Role of histone H3 lysine 27 methylation in Polycomb-group silencing. Science *298*, 1039–1043.

Chambeyron, S., and Bickmore, W.A. (2004). Chromatin decondensation and nuclear reorganization of the HoxB locus upon induction of transcription. Genes Dev. *18*, 1119–1130.

Chambeyron, S., Da Silva, N.R., Lawson, K.A., and Bickmore, W.A. (2005). Nuclear re-organisation of the Hoxb complex during mouse embryonic development. Development *132*, 2215–2223.

Cmarko, D., Verschure, P.J., Otte, A.P., van Driel, R., and Fakan, S. (2003). Polycomb group gene silencing proteins are concentrated in the perichromatin compartment of the mammalian nucleus. J. Cell Sci. *116*, 335–343.

Deschamps, J., and van Nes, J. (2005). Developmental regulation of the Hox genes during axial morphogenesis in the mouse. Development *132*, 2931–2942.

Endoh, M., Endo, T.A., Endoh, T., Fujimura, Y., Ohara, O., Toyoda, T., Otte, A.P., Okano, M., Brockdorff, N., Vidal, M., and Koseki, H. (2008). Polycomb group proteins Ring1A/B are functionally linked to the core transcriptional regulatory circuitry to maintain ES cell identity. Development *135*, 1513–1524.

Endoh, M., Endo, T.A., Endoh, T., Isono, K., Sharif, J., Ohara, O., Toyoda, T., Ito, T., Eskeland, R., Bickmore, W.A., et al. (2012). Histone H2A mono-ubiquitination is a crucial step to mediate PRC1-dependent repression of developmental genes to maintain ES cell identity. PLoS Genet. *8*, e1002774.

Eskeland, R., Leeb, M., Grimes, G.R., Kress, C., Boyle, S., Sproul, D., Gilbert, N., Fan, Y., Skoultchi, A.I., Wutz, A., and Bickmore, W.A. (2010). Ring1B compacts chromatin structure and represses gene expression independent of histone ubiquitination. Mol. Cell *38*, 452–464.

Farcas, A.M., Blackledge, N.P., Sudbery, I., Long, H.K., McGouran, J.F., Rose, N.R., Lee, S., Sims, D., Cerase, A., Sheahan, T.W., et al. (2012). KDM2B links the Polycomb Repressive Complex 1 (PRC1) to recognition of CpG islands. Elife *1*, e00205.

Ficz, G., Heintzmann, R., and Arndt-Jovin, D.J. (2005). Polycomb group protein complexes exchange rapidly in living Drosophila. Development *132*, 3963–3976.

Francis, N.J., Kingston, R.E., and Woodcock, C.L. (2004). Chromatin compaction by a polycomb group protein complex. Science *306*, 1574–1577.

Gao, Z., Zhang, J., Bonasio, R., Strino, F., Sawai, A., Parisi, F., Kluger, Y., and Reinberg, D. (2012). PCGF homologs, CBX proteins, and RYBP define functionally distinct PRC1 family complexes. Mol. Cell *45*, 344–356.

Grau, D.J., Chapman, B.A., Garlick, J.D., Borowsky, M., Francis, N.J., and Kingston, R.E. (2011). Compaction of chromatin by diverse Polycomb group proteins requires localized regions of high charge. Genes Dev. *25*, 2210–2221.

Hernández-Muñoz, I., Taghavi, P., Kuijl, C., Neefjes, J., and van Lohuizen, M. (2005). Association of BMI1 with polycomb bodies is dynamic and requires PRC2/EZH2 and the maintenance DNA methyltransferase DNMT1. Mol. Cell. Biol. *25*, 11047–11058.

Isono, K., Fujimura, Y., Shinga, J., Yamaki, M., O-Wang, J., Takihara, Y., Murahashi, Y., Takada, Y., Mizutani-Koseki, Y., and Koseki, H. (2005). Mammalian polyhomeotic homologues Phc2 and Phc1 act in synergy to mediate polycomb repression of Hox genes. Mol. Cell. Biol. *25*, 6694–6706.

Kessel, M., and Gruss, P. (1991). Homeotic transformations of murine vertebrae and concomitant alteration of Hox codes induced by retinoic acid. Cell *67*, 89–104.

Kim, C.A., Gingery, M., Pilpa, R.M., and Bowie, J.U. (2002). The SAM domain of polyhomeotic forms a helical polymer. Nat. Struct. Biol. *9*, 453–457.

Kmita, M., and Duboule, D. (2003). Organizing axes in time and space; 25 years of colinear tinkering. Science *301*, 331–333.

Ku, M., Koche, R.P., Rheinbay, E., Mendenhall, E.M., Endoh, M., Mikkelsen, T.S., Presser, A., Nusbaum, C., Xie, X., Chi, A.S., et al. (2008). Genomewide analysis of PRC1 and PRC2 occupancy identifies two classes of bivalent domains. PLoS Genet. *4*, e1000242.

Lanzuolo, C., Roure, V., Dekker, J., Bantignies, F., and Orlando, V. (2007). Polycomb response elements mediate the formation of chromosome higher-order structures in the bithorax complex. Nat. Cell Biol. *9*, 1167–1174.

Lavigne, M., Francis, N.J., King, I.F.G., and Kingston, R.E. (2004). Propagation of silencing; recruitment and repression of naive chromatin in trans by polycomb repressed chromatin. Mol. Cell *13*, 415–425.

Miyagishima, H., Isono, K., Fujimura, Y., Iyo, M., Takihara, Y., Masumoto, H., Vidal, M., and Koseki, H. (2003). Dissociation of mammalian Polycomb-group proteins, Ring1B and Rae28/Ph1, from the chromatin correlates with configuration changes of the chromatin in mitotic and meiotic prophase. Histochem. Cell Biol. *120*, 111–119.

Robinson, A.K., Leal, B.Z., Chadwell, L.V., Wang, R., Ilangovan, U., Kaur, Y., Junco, S.E., Schirf, V., Osmulski, P.A., Gaczynska, M., et al. (2012). The growth-suppressive function of the polycomb group protein polyhomeotic is mediated by polymerization of its sterile alpha motif (SAM) domain. J. Biol. Chem. *287*, 8702–8713.

Satijn, D.P.E., and Otte, A.P. (1999). Polycomb group protein complexes: do different complexes regulate distinct target genes? Biochim. Biophys. Acta *1447*, 1–16.

Saurin, A.J., Shiels, C., Williamson, J., Satijn, D.P.E., Otte, A.P., Sheer, D., and Freemont, P.S. (1998). The human polycomb group complex associates with pericentromeric heterochromatin to form a novel nuclear domain. J. Cell Biol. *142*, 887–898.

Sawarkar, R., and Paro, R. (2010). Interpretation of developmental signaling at chromatin: the Polycomb perspective. Dev. Cell *19*, 651–661.

Schwermann, J., Rathinam, C., Schubert, M., Schumacher, S., Noyan, F., Koseki, H., Kotlyarov, A., Klein, C., and Gaestel, M. (2009). MAPKAP kinase MK2 maintains self-renewal capacity of haematopoietic stem cells. EMBO J. *28*, 1392–1406.

Simon, J.A., and Kingston, R.E. (2009). Mechanisms of polycomb gene silencing: knowns and unknowns. Nat. Rev. Mol. Cell Biol. *10*, 697–708.

Solovei, I., Cavallo, A., Schermelleh, L., Jaunin, F., Scasselati, C., Cmarko, D., Cremer, C., Fakan, S., and Cremer, T. (2002). Spatial preservation of nuclear chromatin architecture during three-dimensional fluorescence in situ hybridization (3D-FISH). Exp. Cell Res. *276*, 10–23.

Stamatoyannopoulos, J.A., Snyder, M., Hardison, R., Ren, B., Gingeras, T., Gilbert, D.M., Groudine, M., Bender, M., Kaul, R., Canfield, T., et al.; Mouse ENCODE Consortium. (2012). An encyclopedia of mouse DNA elements (Mouse ENCODE). Genome Biol. *13*, 418.

Stock, J.K., Giadrossi, S., Casanova, M., Brookes, E., Vidal, M., Koseki, H., Brockdorff, N., Fisher, A.G., and Pombo, A. (2007). Ring1-mediated ubiquitination of H2A restrains poised RNA polymerase II at bivalent genes in mouse ES cells. Nat. Cell Biol. *9*, 1428–1435.

Suzuki, M., Mizutani-Koseki, Y., Fujimura, Y., Miyagishima, H., Kaneko, T., Takada, Y., Akasaka, T., Tanzawa, H., Takihara, Y., Nakano, M., et al. (2002). Involvement of the Polycomb-group gene Ring1B in the specification of the anterior-posterior axis in mice. Development *129*, 4171–4183.

Tavares, L., Dimitrova, E., Oxley, D., Webster, J., Poot, R., Demmers, J., Bezstarosti, K., Taylor, S., Ura, H., Koide, H., et al. (2012). RYBP-PRC1 complexes mediate H2A ubiquitylation at polycomb target sites independently of PRC2 and H3K27me3. Cell *148*, 664–678.

Vazquez, J., Müller, M., Pirrotta, V., and Sedat, J.W. (2006). The MCP element mediates stable long-range chromosome-chromosome interactions in Drosophila. Mol. Biol. Cell *17*, 2158–2165.

Wu, X., Johansen, J.V., and Helin, K. (2013). Fbxl10/Kdm2b recruits polycomb repressive complex 1 to CpG islands and regulates H2A ubiquitylation. Mol. Cell *49*, 1134–1146.

Yamaki, M., Isono, K., Takada, Y., Abe, K., Akasaka, T., Tanzawa, H., and Koseki, H. (2002). The mouse Edr2 (Mph2) gene has two forms of mRNA encoding 90- and 36-kDa polypeptides. Gene *288*, 103–110.

Yuan, W., Wu, T., Fu, H., Dai, C., Wu, H., Liu, N., Li, X., Xu, M., Zhang, Z., Niu, T., et al. (2012). Dense chromatin activates Polycomb repressive complex 2 to regulate H3 lysine 27 methylation. Science *337*, 971–975.